Optics Letters

High-power ytterbium-doped fiber laser delivering few-cycle, carrier-envelope phase-stable 100 μJ pulses at 100 kHz

E. Shestaev,[1,*] D. Hoff,[2,3] A. M. Sayler,[2,3] A. Klenke,[1,3] S. Hädrich,[4] F. Just,[4] T. Eidam,[4] P. Jójárt,[5] Z. Várallyay,[5] K. Osvay,[5] G. G. Paulus,[2,3] A. Tünnermann,[1,3,6] and J. Limpert[1,3,4,6]

[1]Friedrich-Schiller-Universität Jena, Abbe Center of Photonics, Institute of Applied Physics, Albert-Einstein-Straße 15, 07745 Jena, Germany
[2]Friedrich-Schiller-Universität Jena, Institut für Optik und Quantenelektronik, Max-Wien-Platz 1, 07743 Jena, Germany
[3]Helmholtz-Institute Jena, Fröbelstieg 3, 07743 Jena, Germany
[4]Active Fiber Systems GmbH, Ernst-Ruska-Ring 11, 07745 Jena, Germany
[5]ELI-ALPS, ELI-HU Non-Profit Ltd., H-6720 Szeged, Dugonics tér 13, Hungary
[6]Fraunhofer Institute for Applied Optics and Precision Engineering IOF, Albert-Einstein-Straße 7, 07745 Jena, Germany
*Corresponding author: evgeny.shestaev@uni-jena.de

Received 6 September 2019; revised 5 November 2019; accepted 11 November 2019; posted 14 November 2019 (Doc. ID 377169); published 18 December 2019

We present a carrier-envelope phase (CEP)-stable Yb-doped fiber laser system delivering 100 μJ few-cycle pulses at a repetition rate of 100 kHz. The CEP stability of the system when seeded by a carrier-envelope offset-locked oscillator is 360 mrad, as measured pulse-to-pulse with a stereographic above-threshold ionization (stereo-ATI) phase meter. Slow CEP fluctuations have been suppressed by implementing a feedback loop from the phase meter to the pulse picking acousto-optic modulator. To the best of our knowledge, this is the highest CEP stability achieved to date with a fiber-based, high-power few-cycle laser.

https://doi.org/10.1364/OL.45.000097

The emerging field of strong-field and attosecond physics [1] has resulted in a demand for lasers with high carrier-envelope phase (CEP) stability. Besides, since many applications in metrology [2], spectroscopy [3], microscopy [4], and physical chemistry [5], to name a few, would strongly benefit from a high photon flux (which ultimately improves the signal-to-noise ratio and shortens the data acquisition time), and there is growing interest in high average power, CEP-stable lasers.

State-of-the-art few-cycle laser systems based on titanium-sapphire (Ti:Sa) regenerative amplifiers, [6–8] as well as optical parametric chirped-pulse amplifiers (OPCPAs) [9,10], have demonstrated a high CEP stability of around 300 mrad which, in rare cases, has even reached the sub-100 mrad range [11–13]. However, the average-power scaling potential of such systems is limited to a few tens of watts due to thermal effects [14,15].

In contrast, chirped pulse amplifiers (CPAs), based on ytterbium-doped fibers (Yb:fiber) have demonstrated their capability in scaling the average power of the emitted radiation to the kilowatt-level and beyond [16] and the pulse energy to the multi-millijoule range [17], but historically they have not shown a high level of CEP stability [18,19]. For example, a Yb-doped fiber laser-driven two-optical-cycle source delivering more than 200 W of average power at a high repetition rate of 1.27 MHz has been demonstrated [20]. Therefore, if the CEP stability is improved, high-power, high-repetition rate fiber lasers will become an ideal source for many applications relying on phase-stable few-cycle pulses. In this context, the question is whether Yb:fiber laser systems are able to produce a highly CEP-stable emission.

This question has been recently answered by the report of a Yb:fiber laser delivering multi-microjoule, multi-10 MHz repetition rate, 30 fs pulses (roughly nine optical cycles) with a very high carrier-envelope offset (CEO) stability of 88 mrad in the frequency range of 0.4 Hz to 400 kHz [21]. Results like this clearly demonstrate the feasibility of achieving a good CEP stability with low peak power fiber laser systems. In the same vein, another very recent report [22] describes a Yb:fiber system seeded by an optical parametric amplifier which delivers 30 μJ, 100 fs pulses (i.e., about 30 optical cycles) at 100 kHz repetition rate with a CEP stability of 375 mrad.

In this Letter, we present a high-performance, sub-8 fs pulse (2.2 cycles) Yb:fiber laser system delivering 100 μJ pulses at a repetition rate of 100 kHz with a CEP stability of 360 mrad which, to the best of our knowledge, is the highest reported to date for this kind of systems. The noise properties of the system are carefully characterized up to half of the pulse repetition rate in a frequency range of 10 Hz to 50 kHz.

The reported system is based on a commercially available Yb:fiber CPA followed by a hollow-core fiber (HCF) compression stage (Fig. 1). The setup is essentially a CEP stability test bed for the ELI-ALPS HR1 and HR2 lasers [23], which are targeting more than an order of magnitude higher pulse energy and average power.

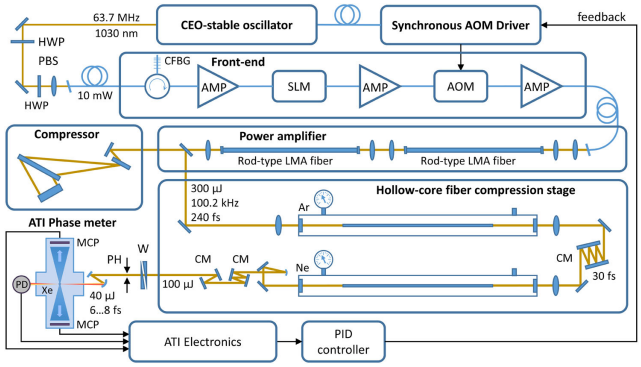

Fig. 1. System description: AMP, amplifier; AOM, acousto-optic modulator; CFBG, chirped fiber Bragg grating; CM, chirped mirror; HWP, half-wave plate; MCP, micro-channel plate; PBS, polarizing beam splitter; PD, photodetector; PH, pinhole; SLM, spatial light modulator; W, wedge pair.

The CEO-stable seed source is a commercial Kerr-lens mode-locked Yb:KGW oscillator, delivering 0.8 W of average power at a pulse repetition rate of 63.7 MHz with an optical bandwidth of 32 nm. About 10 mW of this output radiation are coupled into a delivery fiber (PM980) for seeding the fiber-based CPA system. The all-fiber front end of the system employs polarization-maintaining components, which allow for environmentally stable operation. The pulses are stretched to approximately 700 ps by a chirped fiber Bragg grating. A spatial light modulator (SLM)-based phase shaper is used to improve the pulse quality at the CPA output.

The pulse repetition rate is reduced in the front end to 100 kHz by an acousto-optic modulator (AOM). At this point, it is worth mentioning that any acousto-optic device in a transverse configuration can change the frequency of the light going through it due to the Doppler effect [24]. Such a frequency change directly affects the CEO frequency. This effect can be circumvented with synchronous picking [25] by controlling the frequency of the Doppler shift. The basic idea is to drive the AOM with a harmonic of the pulse repetition frequency. As a result, the optical frequencies of the mode-locked comb lines are shifted by an integer multiple of the pulse repetition frequency, thus maintaining the original CEO frequency f_{ceo} [Fig. 2(a)].

The schematic of the synchronous AOM driver employed in the system is shown in Fig. 2(b). Hereby, the pulse train from the oscillator is detected by a fiber-coupled photodiode (PD), and the 4th harmonic of the repetition rate (f_{rep}) at 254 MHz is then selected by a bandpass filter.

The filtered signal is amplified and fed to a limiter, which stabilizes the output power against amplitude fluctuations of the optical signal. Later on, a low-pass filter is used to remove

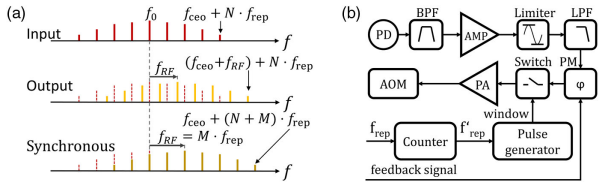

Fig. 2. Synchronous picking. (a) Principle: the RF carrier of the AOM driver is a multiple of the pulse repetition rate, which preserves the CEO frequency of the pulse train. (b) Setup: AMP, amplifier; BPF, bandpass filter; LIM, limiter; LPF, low-pass filter; PA, RF power amplifier; PD, photodiode; PM, phase modulator.

the harmonics that appear after the limiter. The generated RF carrier is sent to a phase modulator to shift its phase, which serves as an actuator for the CEP feedback. Subsequently, the RF carrier is amplitude-modulated by a logical "window" signal that corresponds to the desired pulse repetition rate (f'_{rep}). Finally, a high-power RF amplifier boosts the output power up to approximately 3 W, which is necessary to drive the AOM.

In order to generate a CEP-stable pulse train, the picking factor N should fulfill the equation $N = f_{\mathrm{ceo}}/f'_{\mathrm{rep}} \in \mathbb{N}$. In other words, the ratio of the CEO frequency f_{ceo} of the oscillator to the new pulse repetition rate f'_{rep} should amount to a natural number ($\mathbb{N}$). With the repetition rate f_{rep} of 63.7 MHz and the CEO lock frequency (f_{ceo}) of $f_{\mathrm{rep}}/6$, a picking factor of 636 was selected, resulting in a pulse repetition rate at the CPA output of 100.2 kHz.

The two-stage power amplifier employs rod-type, large mode area large-pitch fibers (LPFs) [26]. The output of the main amplifier is sent to a compressor, which is based on dielectric transmission gratings. The CPA delivers 240 fs, 300 µJ pulses. These pulses are further compressed to 2.2 optical cycles in a two-stage noble gas-filled HCF setup [27]. Both stages employ capillaries with a length of 1 m and an inner diameter of 250 µm. The first stage is filled with argon at 4.5 bars and delivers 190 µJ pulses, which are compressed to 30 fs by chirped mirrors with a total group delay dispersion (GDD) of $-2100\ \mathrm{fs}^2$. The capillary in the second stage is filled with neon at 14.5 bars, which allows obtaining 7.6 fs pulses after a subsequent compression with 2 sets of chirped mirrors. One mirror pair produces a total GDD of $-54\ \mathrm{fs}^2$ to compensate for the dispersion of the 3 mm fused silica laser window, and the second pair has a total GDD of $-67\ \mathrm{fs}^2$. Finally, a pair of wedges was employed for fine adjustment of the dispersion. The output spectrum of the system is shown in Fig. 3(a). The good quality of the compressed pulses is confirmed using both an interferometric autocorrelator [Fig. 3(b)] and the D-Scan measurement [28] [Fig. 3(c)].

First, some sources of phase noise are evaluated to gain an insight into the challenges and to provide an estimation of the lower limit of CEP noise performance of the entire system.

The CEO stability of the oscillator, as well as of the CPA system, was characterized out-of-loop with a fast, high dynamic range f-to-2f interferometer [29]. As can be seen in Fig. 4, the integrated phase noise of the oscillator amounts to 56 mrad in the frequency range from 10 Hz to 21 MHz. The CEO noise of the CPA operating at a pulse repetition rate of 63.7 MHz shows an increased level of high-frequency noise and amounts to 160 mrad, which is a very good result for a high-power laser system.

It is important to note that the AOM was set to constantly transmit the optical pulses, and an attenuation was implemented to mimic the power levels corresponding to operation at 100.2 kHz. The reduction of the pulse repetition rate in the

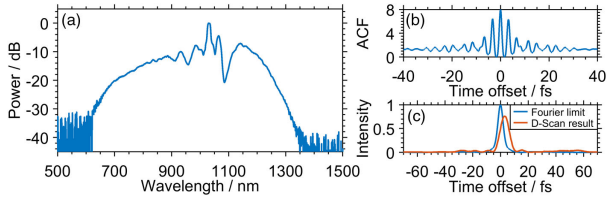

Fig. 3. Spectral and temporal characterization of the output pulses: (a) optical spectrum, (b) interferometric autocorrelation function (ACF), (c) pulse profile retrieved by the D-Scan measurement.

front end of the CPA leads to aliasing of the noise spectrum due to which the high-frequency components are folded onto the lower frequencies. Hence, for a proper comparison, the full information about the CEO noise in the bandwidth of $f_{rep}/2$ is necessary. Thus, by extrapolating the white noise in Fig. 4 up to 31.8 MHz, a total integrated CEO noise of the CPA of 180 mrad is expected.

Since pulse post-compression by means of nonlinear effects demands a high amplitude stability, the conservation of the noise performance cannot be taken for granted. The reason is that the amplitude-to-phase noise coupling [30,31] can quickly lead to noise penalties, even with small amplitude fluctuations at the CPA output. To estimate the excess phase noise induced by amplitude-to-phase noise coupling, the spectral broadening factor due to self-phase modulation for a Gaussian pulse can be calculated by the equation $\Delta\omega_{rms}/\Delta\omega_0 = \sqrt{1 + (4/3\sqrt{3})\phi_{max}^2}$, where $\Delta\omega_{rms}$ is the rms width of the broadened spectrum, $\Delta\omega_0$ is the rms width of the original spectrum, and ϕ_{max} is the maximum accumulated nonlinear phase [32]. The rms spectrum width in our system increases from 5.7 nm at the CPA output to 227 nm after the post-compression stage, resulting in an estimated frequency broadening factor of 45 and a maximum estimated phase shift ϕ_{max} of 51 rad.

This is a key difference to systems starting with shorter pulse durations, such as those presented in Refs. [7,10], or systems using lower compression factors [21,22], since they operate at significantly lower values of the nonlinear phase shift in the spectral broadening stage.

In fact, in the case of high pulse compression factors there are stringent requirements to the amplitude noise of the CPA. For example, in the fiber CPA system described in this Letter, the relative intensity noise (RIN) amounts to 0.13% [Fig. 5(a)] in the frequency range between 10 Hz and 50 kHz. Despite a large spectral broadening factor, the peak excess phase noise induced by coupling via nonlinearity in the HCF compression stage estimates at only 65 mrad due to a remarkably low amplitude noise.

The estimated worst-case CEP performance of the system taking into account the noise measured at the CPA and the excess noise due to amplitude-to-phase coupling in the nonlinear compression stage is 245 mrad. It is worth mentioning that there are other noise sources that are not covered by that analysis, e.g., due to operation of the CPA at higher pulse energies (lower repetition rate) and ionization effects in the post-compression stage.

The CEP noise at the output of the system is measured with a stereographic above-threshold ionization (stereo-ATI) phase meter, capable of single-shot measurement of the absolute phase at repetition rates up to 400 kHz [10]. The pulse energy at the input of the stereo-ATI device was reduced to 40–45 μJ by clipping the beam with a pinhole.

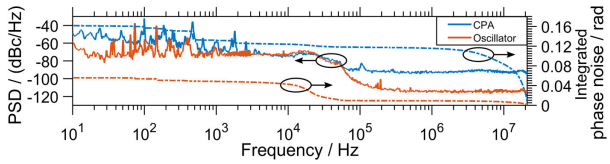

Fig. 4. CEO noise characterization of the CPA and the oscillator performed out-of-loop with an f-to-2f interferometer. The pulse repetition rate for both measurements f_{rep} is 63.7 MHz, and the CEO lock frequency f_{ceo} is 10.6 MHz.

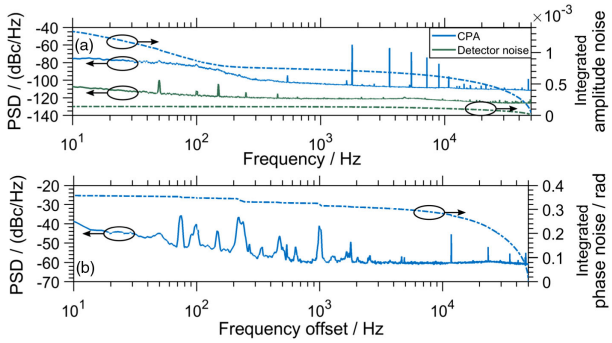

Fig. 5. (a) Amplitude noise of the CPA. The peak at 1.8 kHz and its harmonics are artifacts due to aliasing and were excluded from the analysis. (b) CEP noise of the CPA (only the oscillator is CEO-stabilized).

The measured CEP values are displayed in Fig. 6 as a function of time. The pulse-to-pulse phase fluctuations on a short time scale are shown in Fig. 6(a), whereas a time trace recorded over 10 s is represented as a two-dimensional histogram plot in Fig. 6(b). These plots demonstrate a good short-term stability and a relatively low drift rate of −0.23 rad/s. Figure 6(c) shows a histogram of the CEP values over the 10 s trace, where the linear drift mentioned before has been removed for a better representation of the results. The standard deviation of CEP over 1 million samples is 400 mrad.

The power spectral density (PSD) plot of the CEP noise of the system with only the oscillator CEO-locked is shown in Fig. 5(b). The integrated CEP noise amounts to 360 mrad in the frequency range of 10 Hz to 50 kHz. Only 40 mrad are contributed within 10 Hz to 1 kHz and 40 mrad below 10 Hz (not shown). The largest part is accumulated above 10 kHz due to white noise. This corresponds well with the pulse-to-pulse deviations observed in Fig. 6(a).

The characterization of the CEP noise up to the Nyquist frequency is very important in the presence of white noise and high-frequency contributions. This is only possible by employing single-shot measurement techniques without any averaging of the results, since it would effectively reduce the integration bandwidth and lead to a significant underestimation of the measured noise.

The uncertainty of the measurement by the stereo-ATI phase meter depends on the pulse duration and amplitude stability of the pulse train. In our case, it is estimated at 140 mrad, based on the method described in Ref. [33]. By subtracting the variances, the best-case CEP stability of the system can be estimated to be 330 mrad, which is close to the performance of few-cycle Ti:Sa-based systems [6–8].

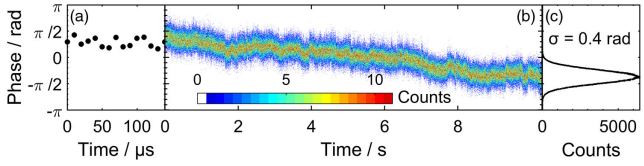

Fig. 6. Evaluation of the CEP stability of the system measured by the stereo-ATI phase meter when only the oscillator is CEO-stabilized: (a) short-term trace over 150 μs, (b) density plot over 10 s, and (c) histogram plot [for best representation, the linear trend of −0.23 rad/s observed in (b) has been removed]. The standard deviation of the CEP is 400 mrad.

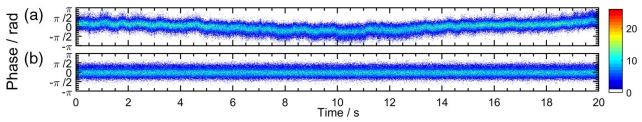

Fig. 7. Density plot of the CEP noise time trace as measured by the stereo-ATI phase meter: (a) when only the oscillator is stabilized and (b) when the "slow loop" feedback is active. False colors: number of counts.

In order to suppress the slow drifts of the carrier-envelope phase due to, e.g., coupling and environmental fluctuations, a feedback loop from the stereo-ATI phase meter to the RF phase modulator in the synchronous picking setup was employed. Figure 7 demonstrates, as a proof of principle, how the slow phase drifts could be completely removed over 20 s. The system maintained in a locked state for several minutes, limited only by the dynamic range of the actuator (2π). Extending the operation time is possible, e.g., by employing an actuator with a higher dynamic range.

To conclude, a compact and robust Yb:fiber laser system delivering 100 μJ, 100 kHz, few-cycle pulses with a CEP stability of 360 mrad in the frequency range of 10 Hz–50 kHz (measured pulse-to-pulse without averaging) is demonstrated. To the best of our knowledge, this is the highest CEP stability reported so far for this kind of systems. Our few-cycle Yb-doped fiber CPA is followed by a HCF nonlinear compression stage, which represents a highly performance-scalable concept. This system offers CEP performance comparable to state-of-the-art Ti:Sa and OPCPA systems. The high stability of the system is achieved in spite of a large frequency broadening factor of 45 in the nonlinear compression stage by employing a CPA with a low amplitude noise of 0.13% RIN (10 Hz–50 kHz). The integrated CEP noise is dominated by broadband, high-frequency noise, showing the importance of noise characterization up to the Nyquist frequency. A feedback loop from the stereo-ATI phase meter to the synchronous picking setup suppressing the slow phase drifts has been demonstrated in a proof-of-principle experiment.

The ongoing research is focused on reducing the white noise content, together with a further optimization of the feedback loop, targeting for an integrated rms noise in the range of 100 mrad. In the near future, it is planned to implement the developed techniques at the ELI-ALPS HR1 and HR2 systems, employing similar components and aiming at more than an order of magnitude higher pulse energy at the same repetition rate. Recently, multi-millijoule, < 10 fs pulses at 300 W of average power delivered by the HR2 laser system have been demonstrated [34].

Funding. Deutsche Forschungsgemeinschaft (SPP-1840 QUTIF); Horizon 2020 Framework Programme (654148); Fraunhofer-Gesellschaft (Cluster of Excellence "CAPS").

Acknowledgment. E. Shestaev acknowledges support by the German Research Foundation (DFG) within the International Research Training Group 2101. The authors thank P. T. Guerreiro and R. Romero from Sphere Ultrafast Photonics for providing the D-Scan device and assistance with the corresponding measurement.

Disclosures. The authors declare no conflicts of interest.

REFERENCES

1. F. Krausz and M. Ivanov, Rev. Mod. Phys. **81**, 163 (2009).
2. T. Udem, R. Holzwarth, and T. W. Hänsch, Nature **416**, 233 (2002).
3. N. Picqué and T. W. Hänsch, Nat. Photonics **13**, 146 (2019).
4. M. I. Stockman, M. F. Kling, U. Kleineberg, and F. Krausz, Nat. Photonics **1**, 539 (2007).
5. M. F. Kling, P. von den Hoff, I. Znakovskaya, and R. de Vivie-Riedle, Phys. Chem. Chem. Phys. **15**, 9448 (2013).
6. D. Adolph, A. M. Sayler, T. Rathje, K. Rühle, and G. G. Paulus, Opt. Lett. **36**, 3639 (2011).
7. F. Lücking, A. Trabattoni, S. Anumula, G. Sansone, F. Calegari, M. Nisoli, T. Oksenhendler, and G. Tempea, Opt. Lett. **39**, 2302 (2014).
8. H. Jacqmin, A. Jullien, B. Mercier, M. Hanna, F. Druon, D. Papadopoulos, and R. Lopez-Martens, Opt. Lett. **40**, 709 (2015).
9. M. Neuhaus, H. Fuest, M. Seeger, J. Schötz, M. Trubetskov, P. Russbueldt, H. D. Hoffmann, E. Riedle, Zs. Major, V. Pervak, M. F. Kling, and P. Wnuk, Opt. Express **26**, 16074 (2018).
10. D. Hoff, F. J. Furch, T. Witting, K. Rühle, D. Adolph, A. M. Sayler, M. J. J. Vrakking, G. G. Paulus, and C. P. Schulz, Opt. Lett. **43**, 3850 (2018).
11. M. Krebs, S. Hädrich, S. Demmler, J. Rothhardt, A. Zaïr, L. Chipperfield, J. Limpert, and A. Tünnermann, Nat. Photonics **7**, 555 (2013).
12. N. Ishii, P. Xia, T. Kanai, and J. Itatani, Opt. Express **27**, 11447 (2019).
13. N. Thiré, R. Maksimenka, B. Kiss, C. Ferchaud, G. Gitzinger, T. Pinoteau, H. Jousselin, S. Jarosch, P. Bizouard, V. Di Pietro, E. Cormier, K. Osvay, and N. Forget, Opt. Express **26**, 26907 (2018).
14. J. Rothhardt, S. Demmler, S. Hädrich, T. Peschel, J. Limpert, and A. Tünnermann, Opt. Lett. **38**, 763 (2013).
15. M. Nisoli, S. Stagira, S. De Silvestri, O. Svelto, S. Sartania, Z. Cheng, M. Lenzner, C. Spielmann, and F. Krausz, Appl. Phys. B **65**, 189 (1997).
16. M. Müller, A. Klenke, A. Steinkopff, H. Stark, A. Tünnermann, and J. Limpert, Opt. Lett. **43**, 6037 (2018).
17. M. Kienel, M. Müller, A. Klenke, J. Limpert, and A. Tünnermann, Opt. Lett. **41**, 3343 (2016).
18. J. Lim, H.-W. Chen, G. Chang, and F. X. Kärtner, Opt. Express **21**, 4531 (2013).
19. L. Pang, H. Han, Z. Zhao, W. Liu, and Z. Wei, Opt. Express **24**, 28993 (2016).
20. S. Hädrich, M. Kienel, M. Müller, A. Klenke, J. Rothhardt, R. Klas, T. Gottschall, T. Eidam, A. Drozdy, P. Jójárt, Z. Várallyay, E. Cormier, K. Osvay, A. Tünnermann, and J. Limpert, Opt. Lett. **41**, 4332 (2016).
21. T. Saule, S. Holzberger, O. De Vries, M. Plötner, J. Limpert, A. Tünnermann, and I. Pupeza, Appl. Phys. B **123**, 17 (2017).
22. M. Natile, A. Golinelli, L. Lavenu, F. Guichard, M. Hanna, Y. Zaouter, R. Chiche, X. Chen, J. F. Hergott, W. Boutu, H. Merdji, and P. Georges, Opt. Lett. **44**, 3909 (2019).
23. ELI-ALPS website, https://www.eli-alps.hu/.
24. B. E. A. Saleh and M. C. Teich, *Fundamentals of Photonics* (Wiley, 1991).
25. O. de Vries, T. Saule, M. Plötner, F. Lücking, T. Eidam, A. Hoffmann, A. Klenke, S. Hädrich, J. Limpert, S. Holzberger, T. Schreiber, R. Eberhardt, I. Pupeza, and A. Tünnermann, Opt. Express **23**, 19586 (2015).
26. J. Limpert, F. Stutzki, F. Jansen, H.-J. Otto, T. Eidam, C. Jauregui, and A. Tünnermann, Light Sci. Appl. **1**, e8 (2012).
27. M. Nisoli, G. Sansone, S. Stagira, C. Vozzi, S. De Silvestri, and O. Svelto, Appl. Phys. B **75**, 601 (2002).
28. M. Miranda, C. L. Arnold, T. Fordell, F. Silva, B. Alonso, R. Weigand, A. L'Huillier, and H. Crespo, Opt. Express **20**, 18732 (2012).
29. A. Klenner, F. Emaury, C. Schriber, A. Diebold, C. J. Saraceno, S. Schilt, U. Keller, and T. Südmeyer, Opt. Express **21**, 24770 (2013).
30. M. Kakehata, Y. Fujihira, H. Takada, Y. Kobayashi, K. Torizuka, T. Homma, and H. Takahashi, Appl. Phys. B **74**, s43 (2002).
31. F. Lücking, V. Crozatier, N. Forget, A. Assion, and F. Krausz, Opt. Lett. **39**, 3884 (2014).
32. G. Agrawal, *Nonlinear Fiber Optics*, 5th ed. (Academic, 2013).
33. T. Wittmann, B. Horvath, W. Helml, M. G. Schätzel, X. Gu, A. L. Cavalieri, G. G. Paulus, and R. Kienberger, Nat. Phys. **5**, 357 (2009).
34. T. Nagy, S. Hädrich, P. Simon, A. Blumenstein, N. Walther, R. Klas, J. Buldt, H. Stark, S. Breitkopf, P. Jojart, I. Seres, Z. Varallyay, T. Eidam, and J. Limpert, Optica **6**, 1423 (2019).